Available online at www.sciencedirect.com

ScienceDirect

Energy Procedia 45 (2014) 1067 – 1076

Energy Procedia

68th Conference of the Italian Thermal Machines Engineering Association, ATI2013

Nusselt correlations in a trailing edge cooling system with long pedestals and ribs

Ahmed Beniaiche[b,c], Carlo Carcasci[a*], Marco Pievaroli[a], Adel Ghenaiet[d]

[a]*Department of Industrial Engineering, University of Florence, via Santa Marta 3 – 50139, Florence, Italy*
[b]*Ecole Militaire Polytechnique, Bordj El Bahri, 16111, Algiers, Algeria*
[c]*Ecole Doctorale d'Energétique et developpement durable, Université Mh'hamed BOUGARA, 35000, Boumerdes, Algeria*
[d]*Université des Sciences et de Technologie Houari Boumediene, 16111, Algiers, Algeria*

Abstract

Detailed TLC measurements have been carried out to estimate the heat transfer coefficient in stationary conditions under high Reynolds numbers in a trailing edge cooling system of a high pressure gas turbine blade. The investigated geometry consists of a 30:1 PMMA scaled model reproducing the typical wedge-shaped discharge duct of a trailing edge cooling system with one row of 7 enlarged pedestals. The section of the channel upstream the pedestal region is used to guide the airflow from the radial hub inlet to the tangential trailing edge outlet; in this section three different surfaces have been studied: one is smooth and the other two are ribbed with +60° and -60° angled ribs respect to the radial direction. This work focuses on the pedestal outlet section, by giving a correlation of the variation of the Nusselt number as a function of the Reynolds number, from 10000 to 40000, in the different inter-pedestal regions along the radial direction. These correlations give the regionally averaged heat transfer coefficients, from the hub to the tip of the model for both smooth and ribbed cases. The interest of these results is the use for the design of the trailing edge blade cooling systems, under the investigated Reynolds number range, that it is the typical case of the industrial application.

Keywords: Trailing edge cooling system; enlarged pedestals; ribs; heat transfer coefficient; thermocromic liquid crystals;

* Corresponding author. Tel.: +39-055-4796245; fax: +39-055-4796342.
E-mail address: carlo.carcasci@unifi.it

doi:10.1016/j.egypro.2014.01.112

1. Introduction

Nowadays, the requirement for more efficient and powerful gas turbines has prompted manufacturers to increase Turbine Inlet Temperature (TIT). However, since the allowable temperatures of the blade material, in modern engines, is far lower than TIT, the need for efficient cooling systems is essential. More than that, in order to reduce weight and improve airfoil efficiency, new casting technologies permit to manufacture blades with very thin trailing edge profiles. The trailing edge of a blade profile is a very thin metallic region subject to heavy mechanical and thermal stresses; this thickness is directly related to the aerodynamic losses. An efficient trailing edge cooling system should maintain blade material under its critical temperature without affecting both mechanical strength and aerodynamic losses. Han et al. [1] gives a widespread review of the used blade cooling technologies. Furthermore, impingement or radial multi-pass channels with ribs cannot be accommodated in the blade trailing edge because of the thin profile, so the most widely used technique to enhance internal heat transfer consists of placing inserts of various shapes, named pedestals, in a slightly converging duct [1]. Circular pin-fin arrays are one of the best technical choices to enhance overall heat transfer coefficient of the coolant in the trailing edge channel. On the other hand, enlarged pedestals have a lengthened shape of the base section, and compared to circular pin fins they increase structural strength, decreasing pressure losses with a limited heat transfer increase. In technical literature, there is a great collection of empirical and numerical analyses concerning pedestal shapes and configurations; several experimental studies were performed to analyze mainly pin-fin cooling capability and related pressure drop. Lau et al. [2, 3] studied the effect of long and short ejection holes on the heat transfer and pressure drop in pin-fin channels. Griffith et al. [4] used low aspect ratio (*AR*) rectangular channels with ribs to enhance the heat transfer. Wright et al. [5] used rectangular channels with pin-fins to study the internal cooling near the trailing edge (*AR*=4:1, and *AR*=8:1). Also others researchers studied pin fins [6, 7, 8, 9]. Carcasci et al. [10] and Facchini et al. [11] determined heat transfer coefficient in a wedge-shaped duct reproducing a trailing edge cooling system with different arrangements of enlarged pedestals and pin fins. Wang et al. [12, 13], using TLC transient technique, performed heat transfer measurements on the endwall surface of pedestal arrays. Also with regard to trailing edge cooling geometries, Hwang and Lui [14, 15] investigated heat transfer and pressure drop in wedge and trapezoidal ducts with different configurations of pin-fin arrays (in-line and staggered) and different outlet flow orientations (straight and turned). Kulasekharan and Prasad [16] performed a wide numerical investigation, testing the effects of flow orientation, channel shape (straight and cambered mean line) and channel section shape (rectangular and convergent). In recent years, numerical and experimental surveys have been addressed to investigate the combined effects of channel shape, blowing tip condition and coolant stream orientation with particular attention to 90° turned ducts to reproduce the mixed axial-radial flow inside gas turbine blades. Bianchini et al. [17, 18] presented an experimental survey on heat transfer coefficient in internal trailing edge ducts. Tests were carried out with steady state TLC technique in order to measure detailed heat transfer coefficient maps over the pressure side endwall. The effects of enlarged pedestals in a wedge shaped duct for a specific trailing edge cooling system have been investigated. Moreover two different blowing tip conditions were studied: with and without blowing tip. Surface and spanwise distributions of heat transfer coefficient show the effect of tip closure; in particular the tip region heat transfer coefficient does not change with Re number. Andrei et al. [19] studied a wedge shaped duct with seven pedestals to drive the flow towards the trailing edge. To replicate the cooling system of the blade in a realistic way, the effect of axial redirection and tip mass flow rate were considered. Later, Bonanni et al. [20] presented a study that is the continuation of a Bianchini's work [18]. The effects of rotation in a radial-axial discharge coolant device of a rotor blade trailing edge have been experimentally evaluated; reference conditions were fixed at Reynolds number *Re*=20000. The results on the pressure side surface are reported in terms of 2D heat transfer distribution maps and spanwise profiles. The performance of three different cases (flat plate, rib orientation of -60° and +60° respect to the radial direction) have been studied in two different coolant discharge conditions: in the first one closed tip outlet presents only axial discharge; instead the second presents a different discharge distribution, where approximately 12.5% of the inlet flow is discharged from the radial tip outlet. For both tip conditions and for the three types of surface (flat or ribbed plate) higher peaks of heat transfer coefficient are shown in stationary cases and are located near the pedestal leading edge and along the pedestal surface facing the approaching flow. These peak values decrease with the increasing of the rotational number for all configurations. Tests show that the rib +60° blowing tip outlet condition reaches the most homogeneous heat transfer distribution all over the heated surface.

Most previous works have focused on the inlet region of the trailing edge cooling cavities, while the inter-pedestal region has not yet been the subject of a detailed analysis. Since this very thin trailing region of the blade profile is subject to heavy thermal and mechanical stresses, a local information of the heat transfer value is necessary in order to avoid premature failure and optimize the cooling of the blade.

The present work is an extended study of Bonanni et al. [20] of an innovative trailing edge geometry. In the present paper: (1) closed tip cases results are presented, (2) the Reynolds number range has been enlarged from 10000 to 40000, (3) trapezoidal ribbed (rib inclination of +60° and -60°) and smooth surfaces are studied (4) and the results are given in terms of heat transfer coefficient maps and Nusselt number correlations versus the Reynolds number ($Nu=C\,Re^n$) for all the studied cases.

Nomenclature

A	Passage Area	[m^2]
AR	Channel aspect ratio	[-]
C	Proportional coefficient of Nusselt correlation	[-]
D	Pedestal width - Diameter	[m]
e	Rib height	[m]
h	Channel height	[m]
H	Heat Transfer Coefficient	[W/m^2K]
k	PMMA thermal conductivity	[W/mK]
m	Mass flow rate	[kg/s]
n	Exponent coefficient of Nusselt correlation	[-]
Nu	Nusselt number	[-]
P	Pedestal or rib pitch	[m]
q	Heat flux	[W/m^2]
Re	Reynolds number	[-]
s	PMMA wall thickness	[m]
T	Temperature	[K]
y	Radial spanwise direction	[m]
μ	Air viscosity	[kg/ms]
α	trailing edge converging angle	[deg]

Acronyms

HTC	Heat Transfer Coefficient
PMMA	PolyMethyl MethAcrylate
TIT	Turbine Inlet Temperature
TLC	Thermochromic Liquid Crystals

Subscripts

a	Air
h	Hydraulic diameter
in	Inlet
L0	Entrance region
L1	Pedestal region
loss	Conduction losses throughout the test section
nat	Natural convection heat transfer
w	Wall
y	Relative on y axis (radial spanwise direction)

2. Experiments

2.1. Experimental apparatus

The experimental survey was performed at the Department of Industrial Engineering at the University of Florence. The test rig consists in an open-loop (ambient pressure) suction type wind tunnel that reproduces a trailing edge internal duct in 30:1 enlarged scale. A high pressure blower (F.lli Ferrari FC 501 N) ensures the coolant flow through the model; before entering the model, air passes through a plenum chamber that allows to set an uniform velocity profile. Air is discharged at ambient pressure through the trailing edge outlet section of the test model.

The coolant mass flow rate is measured by a pressure transducer and a calibrated nozzle, located upstream the blower with a measurement accuracy below 2%.

A pressure scanner Scanivalve DSA 3217, with temperature compensated piezoresistive relative pressure sensors, measures the pressure in 16 different locations in the model with a maximum accuracy of 6.9Pa.

The flow temperature is measured with several T-type thermocouples located in the plenum channel; thermocouples are connected to a data acquisition/switch unit (Agilent 34970A) with a measurement accuracy of 0.5 K.

Surface temperature was evaluated using Thermochromic Liquid Crystals (TLC), hence the model is made of transparent PMMA (Plexiglas®) to assure the optical access. For this purpose wide band TLC 30C20W, supplied by Hallcrest, active from 30°C to 50°C were used. Crystals were thinned down with water and sprayed with an airbrush on the investigated surface. TLC were calibrated in the same optical condition of a real test, moreover the calibration was checked directly on the test article before each experiment. For each test a digital camera (Sony DFW X710) records a color bitmap image (1024x768 pixel) from the TLC painted surface on a PC (IEEE-1394 standard). The illuminating system consists in two studio flashes (DORR DE 500), placed in a steady position on the rig. The heat transfer coefficient is evaluated using the steady state technique: the heating element consists in a 25.4 μm thick Inconel Alloy 600 sheet and is applied on the test plate with a double sided tape. In order to have an uniform heat generation, the heating foil has a rectangular shape and it is connected to two copper bus bars located at hub and tip. Heat flux is controlled by a DC power supplier Agilent N5700.

2.2. Investigated geometry

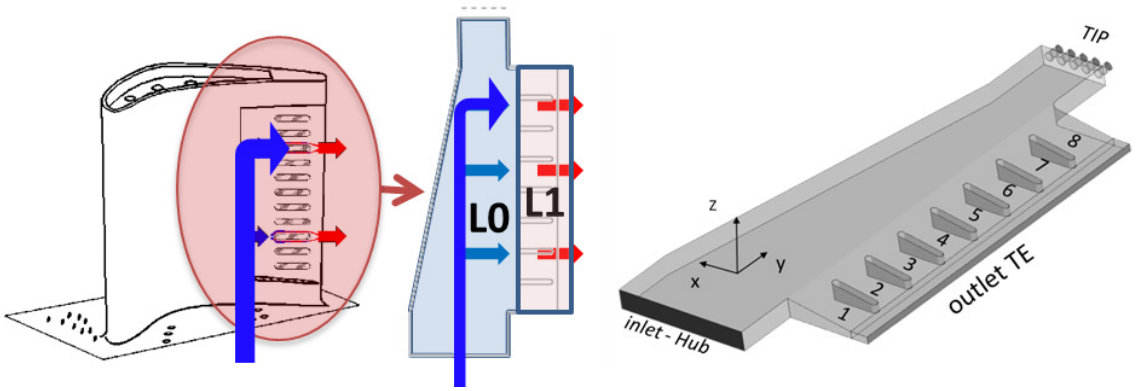

(a) (b)

Fig. 1. Cooling trailing edge scheme (a) and investigated geometry (b)

The investigated geometry (Fig. 1b) reproduces the internal cooling channel of a highly loaded turbine blade, which is the same described and analyzed by Bianchini et al. [18].

The discharge duct at the trailing edge region is wedge shaped and includes a row of seven enlarged pedestals. The cooling air at the inlet section is radially oriented, then is turned by the channel at 90° towards the trailing edge

outlet section. The channel used to guide the flow from the radial inlet to the tangential outlet can be split in 2 parts: the L0 and the L1 region (Fig. 1a).

The L0 region is a constant height channel with a lateral wall that reduces the passage area along the radial y-direction; in this region the coolant flow is redirected towards the trailing edge outlet section. The hub section is a rectangular inlet section, having a hydraulic diameter D_h of 58.18 mm, with an aspect ratio AR of 7.25. Heat transfer measurements on the L0 region surface, which can be used to simulate the pressure side of the blade, were performed in three different configurations. The first one consists in the simple flat plate case and the others consist in two different rib angular orientations: +60° and -60° respect to the radial direction. Ribs are square with 4 mm of height. The distance between two consecutive ribs, called pitch, is the same of the pedestals, i.e. P_y=75.0 mm. The pitch-to-rib height ratio is P_y/e=18.75 and the rib height-to-hydraulic diameter ratio is e/D_h=0.07 for every rib configuration.

The L1 region (Fig. 1a) consists in a converging wedge shaped duct with an initial height h_1=33mm and an angle of inclination α=10°. Seven (7) pedestals are placed inside the L1 region forming eight (8) inter-pedestal regions. These regions are equally spaced at a distance P_y=75.0 mm in the radial direction. Each pedestal has a length of 84.mm and an extreme diameter of 12.mm.

2.3. Experimental procedure and test conditions

Local heat transfer coefficients over the test surface are measured using a steady state technique, evaluating wall temperatures by means of TLC thermography. The parameter used to quantify the color of the painted surface is the hue. A hue calibration of TLC has been performed replicating the same optical conditions of real tests in order to relate color of every pixel location to local wall temperature T_w. During heat transfer tests the surface is heated by a constant thermal flux q that is controlled by the DC power supplier connected to the heating foil. The heated surface is then exposed to the flow and a digital image of the investigated surface is acquired for each Reynolds number.

The Reynolds number for data reduction is calculated in the inlet section (L0) and is defined as:

$$\mathrm{Re} = \frac{m \cdot D_{hL0}}{A_{L0} \cdot \mu_{a,in}} \tag{1}$$

where D_{hL0} is the hydraulic diameter of the inlet duct. Air viscosity $\mu_{a,in}$ is evaluated at the flow temperature measured in the L0 inlet region.

The heat transfer coefficient is defined as:

$$H = \frac{q - q_{loss}}{T_w - T_{a,in}} \tag{2}$$

where T_w represents the wall temperature (measured by TLC), $T_{a,in}$ is the coolant flow temperature and q is the heat flux generated by the Inconel heating foil. This definition also takes into account the thermal losses due to conduction through the solid body. Knowing the thermal conductivity k and the thickness s of PMMA plate, it is possible to evaluate the thermal losses q_{loss} using:

$$q_{loss} = \frac{k}{s} \cdot \frac{T_w - T_{room}}{1 + k/(s \cdot H_{nat})} \tag{3}$$

where T_{room} is the room temperature and H_{nat} is the natural convection heat transfer coefficient evaluated on the external surface of the test model. Thermal losses vary from 3% in low temperature areas up to 10% in high temperature ones. Thus, the full two-dimensional distribution of the heat transfer coefficients is obtained after evaluation.

A total of 12 different tests were performed with varying Reynolds number, from 10000 to 40000, and for the 3 different rib configurations.

2.4. Experimental Uncertainty

The uncertainty analysis was performed following the standard ANSI/ASME PTC 19.1 [21] based on the Kline and Mc-Clintock method [22]. Temperature accuracy is ±0.5 K, differential pressure is ±6.9 Pa, mass flow rate is ±2÷3% while the maximum absolute error is ±10% in measuring the heat transfer coefficient.

3. Results

3.1. HTC maps

Figures 2, 3 and 4 show the heat transfer coefficient maps for different Reynolds numbers (figures from (*a*) to (*d*)) and with different rib configurations (smooth, ribs +60° and ribs -60°) . The color range is the same for each figure. Globally, as it is well note, increasing the Reynolds number, the heat transfer coefficient increases too.

Maps show some peculiar features for every plate, smooth and ribbed +60° and -60° cases but effects are more relevant for high Reynolds numbers (Fig. 2d, 3d and 4d). Two low-HTC value regions are present: the first one is located in the inter-pedestal vane near the hub (ID#01: y/P_y=3.5); the second one is located near the tip along the redirecting wall. For each of these regions, low-HTC value is due to a recirculation bubble. Volumes of these zones (recirculation zones) decrease with the increase of the Reynolds number because more fresh air arrives with the increase of the air velocity; this results in a cooling enhancement of the hot plate at this region.

From maps, it is possible to note that the maximum heat transfer value is reached on the leading edge of each pedestal due to the stagnation point. This effect increases when the Reynolds number is high (it increases from figures (a) with Reynolds of 10000 to figures (d) with Reynolds of 40000). Downstream along the vane, a horse shoe vortex is conveyed along both the pressure and the suction side of the pedestal. This effect is maximum for the second pedestal and decreases along the radial y-direction. The increase of the incidence angle on the leading edge and the consequent recirculating bubble limits the increment of the heat transfer along the suction side.

The acquired figures show that the maximum cooling is localized between the {+2.0, +1.0, 0.0} y/P_y pedestals positions. In the mid pedestal region, a recirculation bubble is developing on the suction side of each pedestal with decreasing extension at higher radii, vice versa an accelerating flow is found on the pressure side where horse-shoe vortices develop in the near wall regions. The outflow at the trailing edge is almost completely axial for the inter-pedestals passage close to the blade hub for which a wide recirculation is affecting the discharge.

In the inter-pedestal vanes, an increment of HTC is present; it develops from the pressure side of the pedestal to the suction side of the previous pedestal. This phenomenon is due to the migration of air from the above pressure side towards the suction side.

As expected, the presence of ribs in the L0 region induces a global heat transfer coefficient enhancement for both +60° and -60° configurations (Fig. 3 and 4). This enhancement brings HTC average value of L0 region close to average value of L1 region. For both ribbed configurations the heat transfer enhancement is lower in the rib leading region than the rib trailing region; this is due to the turbulence generated by the flow separation behind the ribs.

For +60° rib orientation (Fig. 3), it is possible to point out heat transfer peaks near the redirecting wall, where the wall itself boosts the effect of ribs. These peaks are localized in a blade region with no high thermal stress thus, in order to obtain better cooling performance, this rib orientation is not the best.

Moreover, for -60° rib orientation (Fig. 4), the peak values of heat transfer coefficient in the inter-pedestal regions are lower than the flat plate for each Reynolds number. This effect should be explained by the rib orientation towards the axial direction, which decreases the angle of attack of the coolant flow on each pedestal, reducing the global turbulence enhancement due to the pedestals.

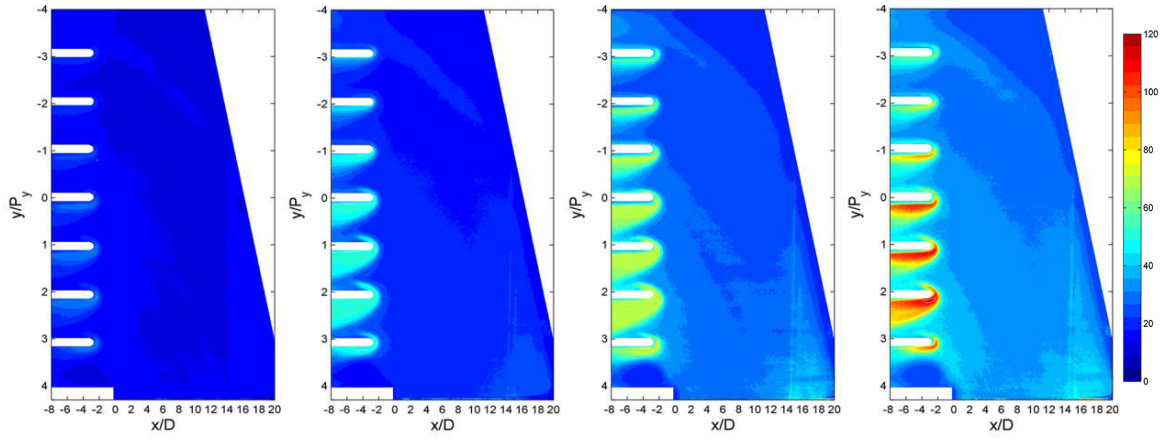

(a) (b) (c) (d)

Fig. 2. HTC maps [W/m^{2}K] for smooth surface for Reynolds 10k (a), 20k (b), 30k (c) and 40k (d)

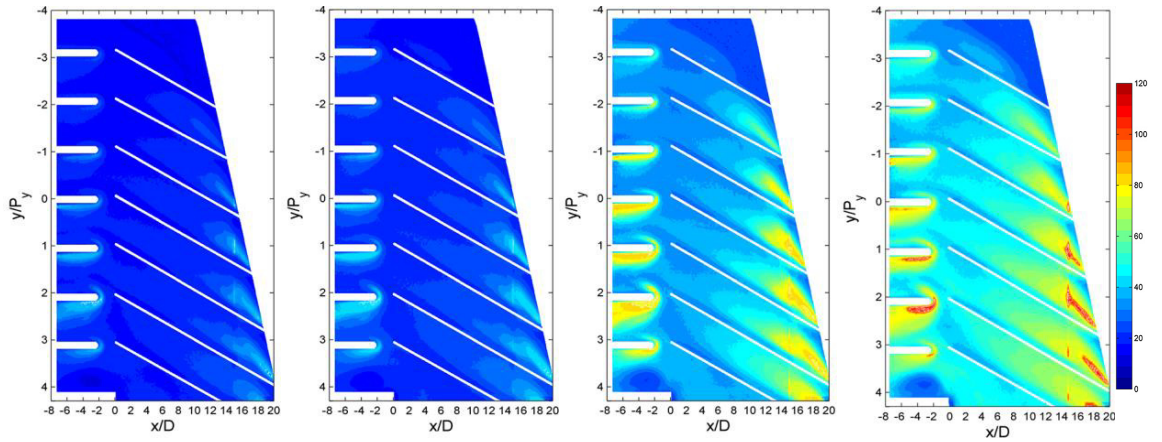

(a) (b) (c) (d)

Fig. 3. HTC maps [W/m^{2}K] with Rib +60° in L0 region for Reynolds 10k (a), 20k (b), 30k (c) and 40k (d)

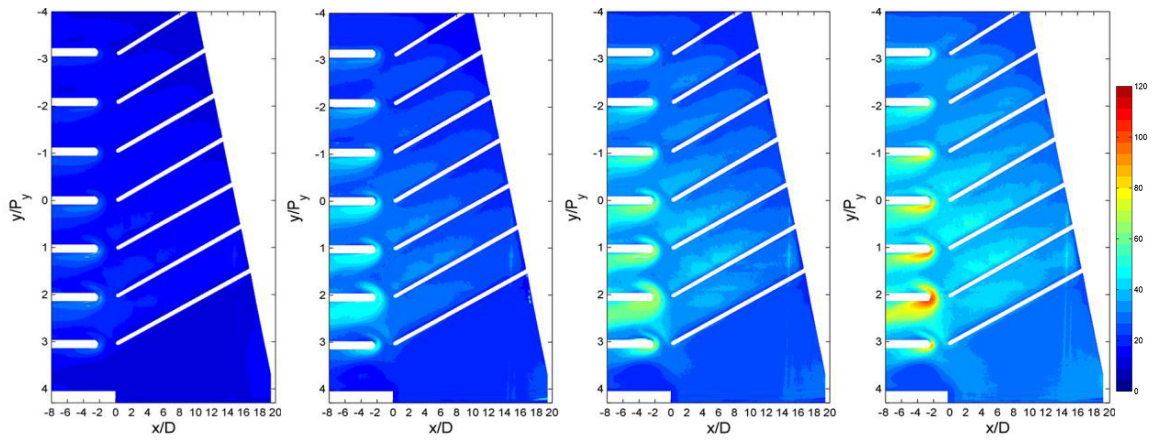

(a) (b) (c) (d)

Fig. 4. HTC maps [W/m^{2}K] with Rib -60° in L0 region for Reynolds 10k (a), 20k (b), 30k (c) and 40k (d)

3.2. Correlations

The correlation of Nusselt number versus Reynolds number is very interesting and useful to design a cooling system. The common Nusselt function is represented by an algebraic expression and generally the following form is used:

$$Nu = C \cdot \mathrm{Re}^{n} \tag{4}$$

The coefficient C and the exponent n of the empirical correlation can be determined from experimental measurement, in fact they are determined minimizing the mean square deviation between the empirical correlation and the experimental results.

The Nusselt number changes for every inter-pedestal, so an average Nusselt number can be determined and the coefficient C and exponent n of correlation can be calculated for each inter-pedestal zone. Figure 5 shows the zones where the Nusselt number is averaged. The L1 inter-pedestal zone is extended 1.0 D (pedestal width) upstream of the pedestals leading edge; this assumption allows to include in this area the HTC peaks described above. In fact, even if the peak occurs in the L0 region, it depends on the presence of the pedestal and has to be charged to the pedestal itself. Figure 6 shows the average Nusselt number in L0 region with and without ribs and the correlation trend lines. The coefficients of Nusselt correlations are shown in Table 1. As expected, the heat transfer coefficient in the smooth case is the minimum value, but a modest high value of HTC is present with -60° ribs configuration, as opposed to +60° ribs configuration which presents the highest HTC values. The exponent n is in the range of 0.65 to 0.70 (see Table 1), which is the accepted range for this kind of experiences regarding the variation of the Nusselt number with the Reynolds number. The results of average Nusselt number in the inter-pedestal areas are presented in Fig. 7 for each studied case (smooth, +60°, -60°) and the correlation coefficients are presented in Table 1. In each case, there is a good agreement with the correlations. For y/P_y=+2.5 (inter-pedestal #02) the highest Nusselt number is present; after this y/P_y position, the coefficient C decreases in the direction of the tip, so the Nusselt number decreases moving from hub (inter-pedestal #02: y/P_y=+2.5), to tip (inter-pedestal #08: y/P_y=-3.5) except the first inter-pedestal (#01: y/P_y=+3.5) where, generally, the Nusselt number is low due to the recirculation bubble.

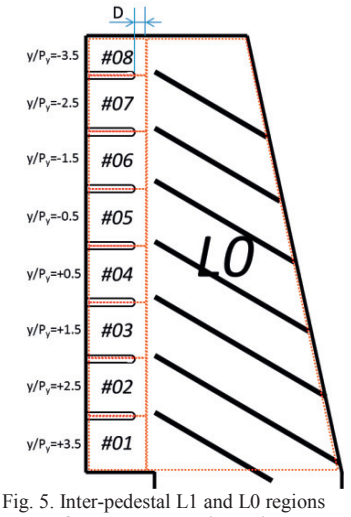

Fig. 5. Inter-pedestal L1 and L0 regions for average Nusselt number

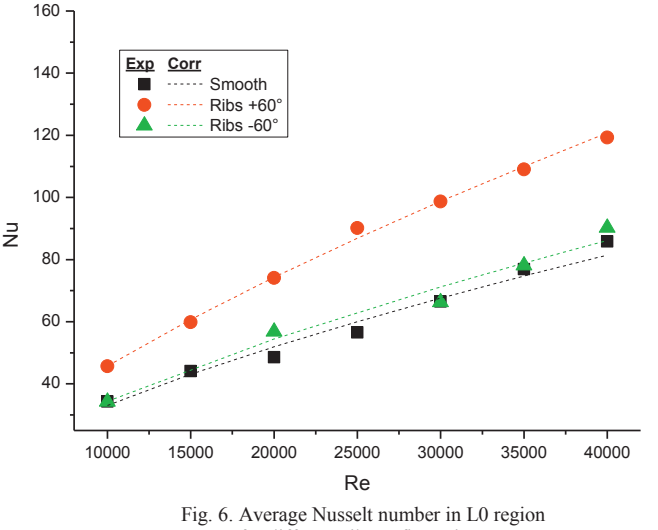

Fig. 6. Average Nusselt number in L0 region for different rib configurations

Comparing the effect of ribs on average Nusselt number of the inter-pedestal regions (Fig. 7a, 7b and 7c), there is not a strong effect. Only in the -60° ribs configuration (Fig. 7c) there is a higher variation from the second to the last pedestal because the ribs position increases the mass flow rate at the tip zone; in fact in this ribs configuration, the Nusselt number in the first inter-pedestal area (#01: y/P_y=+3.5) is the lowest because the recirculation bubble is big.

On the other hand, in the +60° ribs configuration, the recirculation bubble in the first inter-pedestal area is small and so the Nusselt number is higher than the other two configurations, in fact this ribs position favours a more radial uniform mass flow rate.

The main mass flow rates exiting at the trailing edge outlet section are localized at the central part of L1 region [19], so more mass flow rate is localized at y/P_y={+2.5; +1.5; +0.5; -0.5; -1.5} pedestals positions, where air has more passage area and is almost completely axial. The flow is accelerated on the pressure side of the pedestals, where the horse-shoe vortices increase their size in the near wall regions, favouring the cooling in these inter-pedestal positions. Moving from hub to tip the size of the cooled region decreases because of a reduction of mass flow rate and an increasing of air average temperature.

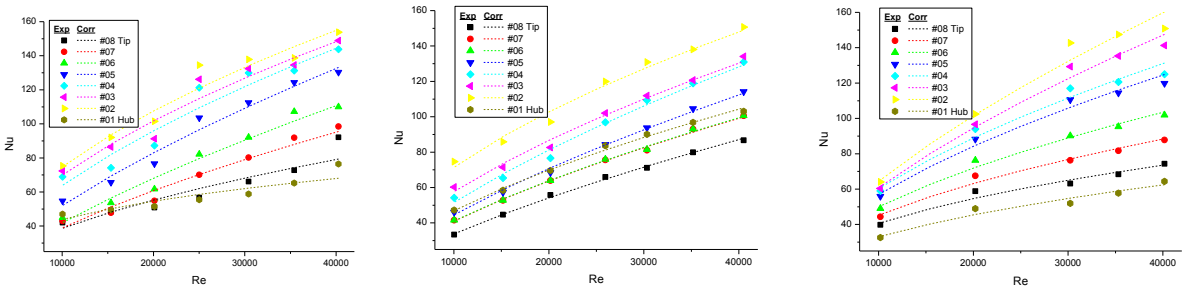

(a) Smooth surface (b) +60° ribbed surface (c) -60° ribbed surface

Fig. 7. Average Nusselt Number versus the Reynolds number in inter-pedestal regions

Table 1. Proportional coefficient *C* and exponent *n* of Nusselt correlation.

interpedestal ID	*y-Position* y/P_y	*Smooth*		*Ribs +60°*		*Ribs -60°*	
		C	*n*	*C*	*n*	*C*	*n*
L0 region	---	0.0831	0.6500	0.0720	0.7007	0.0771	0.6624
08 (Tip)	-3.5	0.3312	0.5167	0.0617	0.6844	0.7787	0.4292
07	-2.5	0.1013	0.6460	0.1151	0.6378	0.5269	0.4833
06	-1.5	0.0653	0.7017	0.1145	0.6386	0.3929	0.5260
05	-0.5	0.1028	0.6759	0.0944	0.6683	0.3163	0.5639
04	0.5	0.2765	0.5906	0.1203	0.6579	0.3498	0.5592
03	1.5	0.4672	0.5436	0.2548	0.5886	0.1696	0.6385
02	2.5	0.5857	0.5264	0.5598	0.5263	0.1536	0.6556
01 (Hub)	3.5	2.3992	0.3155	0.2294	0.5775	0.4829	0.4588

4. Conclusion

In the present work, the heat transfer characteristics of a wedge-shaped discharge duct of a trailing edge cooling system are investigated. Steady heat transfer measurements using TLC are carried out both in the channel upstream the pedestal zone (L0 region) and in the outlet pedestal section (L1 region). In particular local distributions of the Nusselt number are obtained as a Reynolds number function at the different inter-pedestals regions along the radial direction. The performance of three different rib configurations (smooth, ribs +60° and ribs -60°) in the L0 region are investigated varying the Reynolds number at the hub section from 10000 to 40000 in closed tip condition. In each case, two low-HTC value regions are present: the first one is located in the inter-pedestal vane near the hub; the second one is located near the tip along the redirecting wall.

Concerning L0 region the +60° ribs configuration improves the heat transfer phenomena and ensures the highest heat transfer enhancement. The ribs, in addition to increase the heat transfer coefficient in the L0 region, present an effect on recirculation bubble and, thus, on low-HTC zone.

Concerning L1 region the Nusselt number decreases moving from hub to tip except the first inter-pedestal zone where, generally, the Nusselt number is low. In this case the flat plate (without ribs) presents slightly higher values of heat transfer coefficient compared to the ribbed configurations; this is more evident between the {+2.0, +1.0, 0.0} y/P_y pedestals positions.

A heat transfer correlation for each inter-pedestal area and for the main region is determined. A good agreement between correlation and experimental data is found. The exponent of Nusselt number correlation is between 0.5 to 0.7 that is the accepted range for this kind of experiences.

Acknowledgements

The reported work has been supported by the Italian Ministry of Education, University and Research (MIUR). Authors would also gratefully thank Prof. Bruno Facchini for his great effort of supervisor.

References

[1] Han J.C., Dutta S., Ekkad S.V. *Gas Turbine Heat Transfer and Cooling Technology*. First ed. New York: Taylor & Francis; 2000.
[2] Lau S.C., Han J.C., Batten T. Heat Transfer, Pressure Drop, and Mass Flow Rate in Pin Fin Channels with Long and Short Trailing Edge Ejection Holes. *ASME Journal of Turbomachinery* 1989; Vol. III:116-122.
[3] Lau S.C., Han J.C., Batten T. Turbulent Heat Transfer and Friction in Pin Fin Channels with Lateral Flow Ejection. *ASME Journal of Heat Transfer* 1989; Vol. III:51-58.
[4] Griffith T.S., Al-Hadhrami L., Han J.C. Heat transfer in rotating rectangular cooling channel (AR=4) with dimples. *ASME Paper* 2002; GT–2002–30220.
[5] Wright L.M., Fu W.L., Han J.C. Thermal Performance of Angled, V-Shaped, and W-Shaped Rib Turbulators in Rotating Rectangular Cooling Channels (AR=4:1*). ASME Journal of Turbomachinery* 2004; 126(4):604-614.
[6] Metzger D.E., Berry R.A., Bronson J.P. Developing heat transfer in rectangular ducts with staggered arrays of short pin fins. *ASME Journal of Heat Transfer* 1982; 104(1):700-706.
[7] Metzger D.E., Haley S.W. Heat transfer experiments and flow visualization for arrays of short pin fins. *ASME Paper* 1982; 82-GT-138.
[8] Metzger D.E., Shepard W.B., Haley S.W. Row resolved heat transfer variations in pin-fin arrays including effects of non-uniform arrays and flow convergence. *ASME Paper* 1986; 86-GT-132.
[9] Hwang J.J., Lui C.C. Measurements of endwall heat transfer and pressure drop in a pin-fin wedge duct. *International Journal of Heat and Mass Transfer* 2002; 45:877-889.
[10] Carcasci C., Facchini B., Innocenti L. Heat transfer and pressure drop evaluation in thin wedge-shaped trailing edge. *ASME Paper* 2003; GT2003-38197.
[11] Facchini B., Innocenti L., Tarchi L. Pedestal and endwall contribution in heat transfer in thin wedge shaped trailing edge. *ASME Paper* 2004; GT2004-53152.
[12] Wang Z., Ireland P.T., Jones T.V. Detailed heat transfer coefficient measurements and thermal analysis at engine conditions of a pedestal with fillet radii. *ASME Paper* 1993; 93-GT-329.
[13] Wang Z., Ireland P.T., Jones T.V., Kohler S.T. Measurements of local heat transfer coefficient over the full surface of a bank of pedestals with fillet radii. *ASME Paper* 1994; 94-GT-307.
[14] Hwang J.J., Lui C.C. Measurement of endwall heat transfer and pressure drop in a pin-fin wedge duct. *International Journal of Heat and Mass Transfer* 2002; 45:877–889.
[15] Hwang J.J., Lui C.C. Detailed heat transfer characteristic comparison in straight and 90-deg turned trapezoidal ducts with pin-fin arrays. *International Journal of Heat and Mass Transfer* 1999; 42:4005–4016.
[16] Kulasekharan N., Prasad B.V.S.S.S. Effect of coolant entry orientation on flow and heat transfer in trailing region channels of a gas turbine vane. *ASME Paper* 2008; GT2008-50343.
[17] Bianchini C., Facchini B., Simonetti F., Tarchi L. Numerical and experimental investigation of turning flow effects on innovative pin fin arrangements for trailing edge cooling configurations. *ASME Paper* 2010; GT2010-23536.
[18] Bianchini C., Bonanni L., Carcasci C., Facchini B., Tarchi L. Experimental survey on heat transfer in an internal channel of a trailing edge cooling system. *65° Associazione Termotecnica Italiana National Conference* 2010; 12_085.
[19] Andrei L., Andreini A., Bonanni L., Facchini B. Heat Transfer in internal channel of a blade: effects of rotation in a trailing edge cooling system. *10th International Symposium on Experimental Computational Aerothermodynamics of Internal Flows* 2011.
[20] Bonanni L., Carcasci C., Facchini B., Tarchi L. Experimental survey on heat transfer in a trailing edge cooling system: effects of rotation in internal cooling ducts. *ASME Paper* 2012; GT2012-69638.
[21] ASME. Measurement uncertainty. In *Instrument and Apparatus*, volume ANSI/ASME PTC 19.1-1985 of Performance Test Code 1985.
[22] Kline S.J., McClintock F.A. Describing uncertainties in single sample experiments. *Mechanical Engineering* 1953; 75:3–8.